Thermal Contraction and Disordering of the Al(110) Surface

Nicola Marzari,[1,*] David Vanderbilt,[1] Alessandro De Vita,[2,3] and M. C. Payne[4]
[1]*Department of Physics and Astronomy, Rutgers University, Piscataway, New Jersey 08854-8019*
[2]*INFM and Department of Material Engineering and Applied Chemistry, University of Trieste, I-34149 Trieste, Italy*
[3]*Institut Romand de Recherche Numérique en Physique des Matériaux, PPH-Ecublens, CH-1015 Lausanne, Switzerland*
[4]*Cavendish Laboratory (TCM), University of Cambridge, Madingley Road, Cambridge CB3 0HE, England*
(Received 16 June 1998)

Al(110) has been studied for temperatures up to 900 K via ensemble density-functional molecular dynamics. The strong anharmonicity displayed by this surface results in a negative coefficient of thermal expansion, where the first interlayer distance decreases with increasing temperature. Very shallow channels of oscillation for the second-layer atoms in the direction perpendicular to the surface support this anomalous contraction, and provide a novel mechanism for the formation of adatom-vacancy pairs, preliminary to the disordering and premelting transition. Such characteristic behavior originates in the free-electron-gas bonding at a loosely packed surface. [S0031-9007(99)08925-5]

PACS numbers: 68.35.Ja, 65.70.+y, 68.45.Gd, 71.15.Pd

Metal surfaces exhibit a remarkable behavior as a function of the temperature. Thermodynamic stability is often determined by a delicate balance between energetic and entropic effects, and can lead to a rich phenomenology for the phase diagrams of different systems. Unreconstructed face-centered cubic (110) surfaces (e.g., Al, Cu, Ni) display a damped oscillatory pattern of interlayer relaxations, starting with a large contraction between the first and the second layers [1,2]. Such behavior originates in the response of surface atoms to undercoordination: moving towards the underlying layer, they increase their surrounding charge density while reducing the corrugation of the surface and the lateral tensile strain [3]. When the temperature is raised, this undercoordinated layer can start to disorder even before the melting temperature of the bulk is reached. While the suggestion that a surface could act as a nucleation stage for melting had long been made, experimental evidence of a reversible melting transition limited to the outer surface layers came only recently [4]. For the case of Al(110), several experimental techniques (ion blocking and shadowing, electron or neutron diffraction, He scattering) have since shown a clear onset of disordering at temperatures between 770 and 815 K [5], whereas the bulk melting temperature is 933 K. Computer simulations based on different models (effective-medium theory [6,7], embedded-atom method [8], glue models [9]) have then been applied to the study of several (110) surfaces (Pb, Al, Cu, Ni), and surface premelting was observed in all cases.

However, many issues remain unresolved. Extensive low-energy electron diffraction (LEED) studies in Al(110) [1(c)] show a *negative* thermal expansion coefficient for the first interlayer distance, and a large positive one (twice the bulk value) for the second interlayer distance. These findings are at variance with widely held general theoretical considerations [10], and with the results of available computer simulations for Cu, Ni, and Al [7–9] which predict an expansion of the first interlayer distance with temperature. In addition, model calculations fail to reproduce the zero-temperature multilayer relaxation pattern [7,8], predicting only the contraction of the first interlayer. On Al(110) the premelting transition is preceded by an anomalous proliferation of adatoms on the surface [5], for which there is no reliable microscopic picture. Finally, the degree of anharmonicity and anisotropy of the different surface layers, as opposed to the bulk, is not known, due to the experimental difficulty in resolving different layers.

Ab initio molecular dynamics (MD) simulations of metal surfaces are very challenging, and only a few and limited studies have been attempted. We use here an approach that we recently introduced [11,12] [ensemble density-functional theory (eDFT)], together with a technical improvement for the Brillouin zone integrations (so-called "cold smearing"), which is particularly suited to MD simulations. Applying this scheme to the case of Al(110), we provide the first theoretical confirmation of a negative thermal expansion for this surface, and excellent agreement with the experiments for the temperature-dependent multilayer relaxations. Moreover, we present a novel, and in retrospect simple, picture of the microscopic mechanisms that lead to this anomalous thermal contraction and to the surface disordering associated with premelting.

In first-principles calculations for metals it is customary to introduce a fictitious electronic temperature σ [13,14], to broaden the density of states and to smooth the discontinuities at the Fermi energy μ, greatly improving the sampling accuracy of a given set of k points. It is very convenient to choose a broadening that has zero first and second moments, so that the resulting electronic free energy does not have any quadratic dependence on the broadening temperature, and neither do its derivatives with respect to any external parameter [12,15] (e.g., the Hellmann-Feynman forces, or the stress tensor). In the existing schemes this is achieved at the price of allowing for *negative* orbital occupancies [15], so that problems can arise in self-consistent calculations where

 0031-9007/99/82(16)/3296(4)$15.00

the total electronic density may become negative. Here, we present a broadening scheme leading to an occupation function that is *positive* definite. Occupation broadening convolutes the density of states with a broadening of the δ function [13,14]; the cold-smearing broadening is

$$\tilde{\delta}(x) = \frac{2}{\sqrt{\pi}} e^{-[x-(1/\sqrt{2})]^2} (2 - \sqrt{2}\, x). \quad (1)$$

Spin degeneracy is assumed here, and $x = \frac{\mu - \epsilon}{\sigma}$. The "generalized entropic functional" $S = \sum_i s_i$ that can be derived [13] and the occupation numbers $f_i = \int_{-\infty}^{x_i} \tilde{\delta}(x)\, dx$ can all be expressed in terms of pseudoenergies $\tilde{\epsilon}_i$ [16] ($x_i = \frac{\mu - \tilde{\epsilon}_i}{\sigma}$); in particular,

$$s_i = \frac{1}{\sqrt{\pi}} e^{-[x_i-(1/\sqrt{2})]^2} (1 - \sqrt{2}\, x_i). \quad (2)$$

No practical difficulty to the self-consistent calculations is caused by the fact that some spin-degenerate occupancies can still exceed 2; this was also the case for the choices set forth in Ref. [15].

The calculations use the local-density approximation (LDA) and norm-conserving pseudopotentials, with a plane-wave basis cutoff of 11 Ry. The bulk properties of Al are well represented: the lattice parameter is 3.96 (4.02) Å, the elastic constants $C_{11} = 117$ (114) GPa, $C_{12} = 66$ (62) GPa, and $C_{44} = 39$ (32) GPa (experimental results at 0 K [17] are in parentheses). The simulation cell is a 3×3 eight-layer Al(110) slab, containing 72 atoms separated by 8.5 Å of vacuum. k-point sampling is performed with the $\frac{1}{4}, \frac{1}{4}, \frac{1}{4}$ Baldereschi point, using $\sigma = 0.5$ eV of cold smearing.

The zero-temperature structural properties are summarized in Table I: good and consistent agreement with the experimental results is registered. The eight-layer calculation has been performed using the same finite cell and sampling of the MD simulations; this introduces some small finite-size errors that can be evaluated exactly at 0 K comparing them with a fully converged calculation (a 1×1 fifteen-layer slab with $12 \times 12 \times 2$ k-point sampling).

Constant-temperature MD simulations have been performed using a Gaussian thermostat and a leapfrog velocity Verlet algorithm to integrate the ionic equations of motion [18], using a time step of 8 fs. A set tolerance for each time step of 5 meV/cell in the spread of the total energies over the last five electronic iterations resulted in a negligible drift of the constant of motion [less than 1.5 (meV/atom)/ps for a microcanonical run]. The lattice parameter parallel to the surface was fixed applying the experimental thermal expansion coefficient for the bulk to the LDA equilibrium lattice parameter. We followed five runs, at increasing temperatures of 400, 600, 700, 800, and 900 K, for 5, 10, 6, 6, and 6 ps, respectively.

TABLE I. Theoretical and experimental values for the interlayer relaxations in Al(110); theoretical values are at 0 K.

	d_{12}	d_{23}	d_{34}	d_{45}
LDA, 8 layers	−6.1%	+5.5%	−2.2%	+1.7%
LDA, 15 layers	−7.4%	+3.8%	−2.5%	+2.0%
LEED[a] (100 K)	−8.6%	+5.0%	−1.6%	
LEED[b] (70 K)	−6.9%	+4.1%	−3.7%	+1.7%

[a]Reference [1(a)].
[b]Reference [1(c)].

We present in Fig. 1 our results for the mean square displacements (MSDs) in the different layers, from the surface to the interior of the crystal, during a 5 ps run at 400 K. The horizontal scale shows the decremental time: the plot starts with the averages over the full run, then proceeds by discarding a progressively longer initial segment. This approach highlights the initial thermalization time (negligible in this case) and the flatness of the plateau for the converged time average, and provides an estimate for the statistical errors. The left panel of Fig. 1 shows the [001] component for the MSDs (we label it x); this component is parallel to the surface and perpendicular to the $[\bar{1}10]$ rows that characterize the (110) surface. The right panel shows the [110] z component, perpendicular to the surface. The time averages are well converged, with the third- and fourth-layer results very close to each other (giving us confidence on the absence of finite-size effects), and close to the experimental bulk values [19].

Two results stand out from the simulation. First, the MSDs in the x direction are twice as large for the surface atoms than for those in all the other inner layers. While it can be expected that the undercoordinated atoms on the surface should be more loosely bound, the large difference

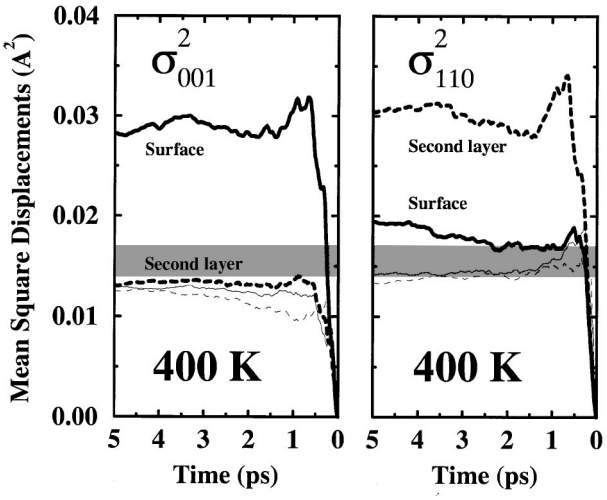

FIG. 1. Layer-resolved mean square displacements at 400 K; left panel shows the [001] components (henceforth labeled x), the right panel the [110] ones (z). The third- and fourth-layer data are given by the unlabeled solid and dashed thin lines. The shaded area corresponds to the bulk experimental values of Ref. [19]. The horizontal axis shows the time over which averaging was performed.

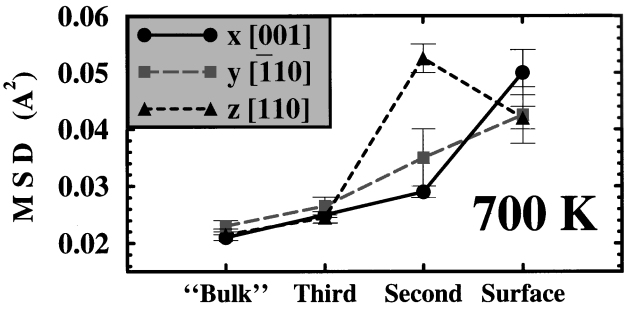

FIG. 2. Layer-resolved mean square displacements at 700 K. The x, y ones parallel to the surface are in solid black and dashed grey (x is perpendicular and y is parallel to the $[\bar{1}10]$ rows); the z ones, perpendicular to the surface are in dashed black. "Bulk" refers to the two inner layers.

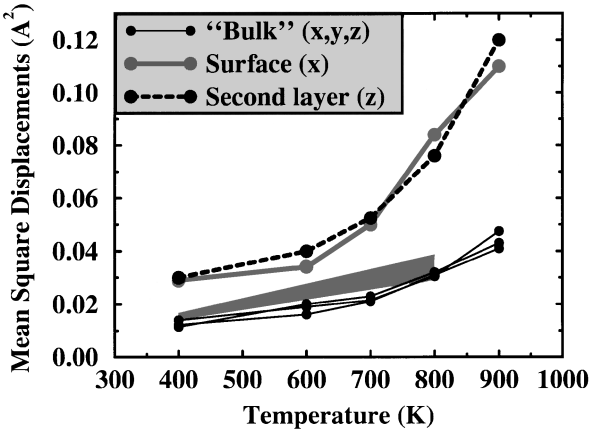

FIG. 3. Layer-resolved mean square displacements as a function of temperature. The shaded area corresponds to the bulk experimental values of Ref. [19].

with the averages for the lower layers is notable. Second, the MSDs in the z direction (i.e., perpendicular to the surface) are *much larger in the second layer than in the first layer.* This is a distinctive feature of this crystallographic orientation that was first encountered in embedded-atom simulations of Ni(110) and Cu(110) [8]. In Al the effect is more striking due to its free-electron-gas behavior. A simple rationalization can be offered: since the (110) surface is very open, atoms in the second layer have natural channels of oscillation perpendicular to the surface and directed towards the vacuum. The charge density on the top of the second-layer atoms is still quite homogeneous, and the bonds are easily stretched, thus leaving the freedom for the atoms to move back and forth along these channels. On the other hand, atoms in the first (surface) layer see the vacuum acting as a hard wall, limiting their mobility outwards; their largest oscillations are thus parallel to the surface and perpendicular to the $[\bar{1}10]$ rows.

The anisotropic behavior of the surface dynamics can be gauged by looking at Fig. 2, where the MSDs at 700 K are plotted in all three crystallographic orientations as a function of the layer depth. Moving from the bulk to the surface, one can observe that the third layer still behaves in a bulklike fashion: the MSDs are isotropic, and they are only slightly larger than those in the two layers below. The anisotropy becomes very distinct in the second layer, with its characteristic large MSDs perpendicular to the surface, and persists in the first layer, for which the "easy" channels are parallel to the surface and across the close-packed $[\bar{1}10]$ rows. Some of the components for the MSDs in the first and second layers can be up to 2–3 times their bulk counterparts. These enhancements near the surface are due to the lower coordination; in addition, a higher degree of anharmonicity makes these surface MSDs increase much more rapidly with temperature than the bulk ones. This becomes apparent from the plot in Fig. 3 of the MSDs as a function of the temperature. The innermost layers show isotropic MSDs, with some deviation from the linear regime only above 700 K (in the harmonic regime the MSDs dependence on the temperature is exactly linear). The outer layers, on the contrary, are strongly anharmonic. The very large increases in the vibrational amplitudes along the easy channels are precursors to the creation of adatoms and vacancies on the surface that lead to the disordering and premelting of the surface. In fact, we observe that with increasing temperature atoms in the second layer start making increasingly large slow excursions towards the surface. One of these events is shown in Fig. 4; the highlighted atom temporarily pops out from the surface. In another event the second-layer atom remained outside the surface, creating an adatom-vacancy pair where the vacancy is initially in the second layer (this void is quickly filled up by a surface atom). In this second case the adatom diffused away via exchange diffusion.

The microscopic dynamics provides a clear explanation of the behavior of this surface that displays an increasing contraction of the first interlayer distance with temperature, where a large expansion would have been expected. The contraction can be understood looking at the motion of the second-layer atoms along these channels that are shallower towards the vacuum. With increasing temperature, the center of mass of the second layer moves outwards, since it is not hampered by nearest neighbors directly on top (the first layer is staggered with respect

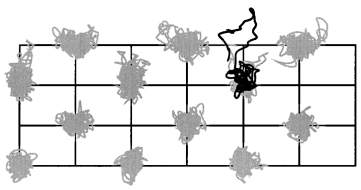

FIG. 4. Projected view of the MD trajectories in the $(\bar{1}10)$ plane, for the top four layers of the slab. The large excursion towards the surface of a second-layer atom has been highlighted.

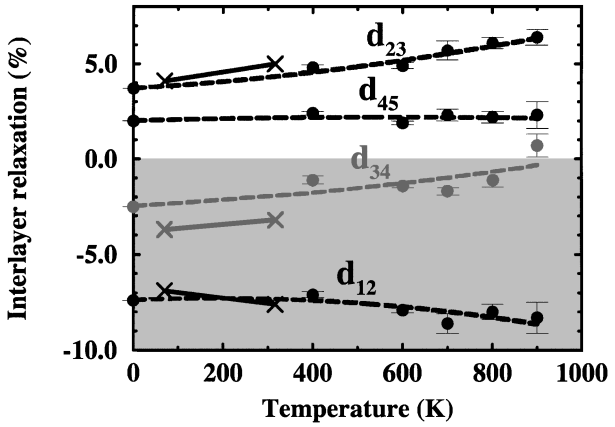

FIG. 5. Interlayer relaxations as a function of temperature. Solid circles: eDFT MD simulations, with their statistical error bars; dashed lines: quadratic least-squares fit; crosses: experimental LEED values (Ref. [1(c)]). The eDFT data have had their 0 K finite-size corrections added rigidly at all temperatures.

to the second). The first layer is more limited in its expansion, since the vacuum acts as a hard wall. The end result is that the average distance between the first and the second layers decreases with temperature. This decrease is then offset by a larger thermal increase of the distance between the second and the third layers. The results of our simulations for the interlayer relaxation as a function of temperature (see Fig. 5) are in very good quantitative agreement with the LEED data (Ref. [1(c)]).

In conclusion, our calculations on Al(110) represent the first extensive first-principles molecular-dynamics simulations of the dynamics on a metal surface, presenting both an insightful picture of the microscopic dynamics and a remarkable agreement with the available experimental data. The microscopic dynamics of this surface is peculiar, and governed by the interplay between the free-electron-gas behavior of the bulk and the quasicovalent bonding of the undercoordinated surface atoms. Two distinct soft channels of oscillation have been identified. One channel is at the surface in the [001] direction, perpendicular to the close-packed surface grooves. The other, unexpected, is perpendicular to the surface but confined to the second-layer atoms. It is this channel that is responsible for the observed anomalous contraction of the surface with temperature. Additionally, it provides a novel, favored mechanism for the generation of adatom-vacancy pairs, whose proliferation is a precursor to the disordering and premelting transition.

N. M. acknowledges support by NSF Grant No. DMR-96-13648; these calculations have been performed on the Hitachi S3600 at the University of Cambridge High Performance Computing Facility.

*Present address: Center for Computational Materials Science, Naval Research Laboratory, Washington, D.C.

[1] (a) J. N. Andersen, H. B. Nielsen, L. Petersen, and D. L. Adams, J. Phys. C **17**, 173 (1984); (b) J. R. Noonan and H. L. Davis, Phys. Rev. B **29**, 4349 (1984); (c) H. Göbel and P. von Blanckenhagen, *ibid.* **47**, 2378 (1993).

[2] K.-M. Ho and K. P. Bohnen, Phys. Rev. B **32**, 3446 (1985).

[3] M. W. Finnis and V. Heine, J. Phys. F **4**, L37 (1974); R. J. Needs, M. J. Godfrey, and M. Mansfield, Surf. Sci. **242**, 215 (1991); P. J. Feibelman, Phys. Rev. B **51**, 17 867 (1995); J.-H. Cho *et al.*, Phys. Rev. B **59**, 1677 (1999).

[4] J. W. M. Frenken and J. F. van der Veen, Phys. Rev. Lett. **54**, 134 (1985).

[5] A. W. Denier van der Gon, R. J. Smith, J. M. Gay, D. J. O'Connor, and J. F. van der Veen, Surf. Sci. **227**, 143 (1990); H. Dosch, T. Höfer, J. Peisl, and R. L. Johnson, Europhys. Lett. **15**, 527 (1991); A. Pavlovska, M. Tikhov, Y. Gu, and E. Bauer, Surf. Sci. **278**, 303 (1992); M. Polčik, L. Wilde, and J. Haase, Phys. Rev. Lett. **78**, 491 (1997).

[6] P. Stoltze, J. K. Norskøv, and U. Landman, Phys. Rev. Lett. **61**, 440 (1988); Surf. Sci. **220**, L693 (1989); H. Häkkinen and M. Manninen, Phys. Rev. B **46**, 1725 (1992).

[7] P. D. Ditlevsen, P. Stoltze, and J. K. Norskøv, Phys. Rev. B **44**, 13 002 (1991); P. D. Ditlevsen and J. K. Norskøv, Surf. Sci. **254**, 261 (1991).

[8] E. T. Chen, R. N. Barnett, and U. Landman, Phys. Rev. B **41**, 439 (1990); R. N. Barnett and U. Landman, *ibid.* **44**, 3226 (1991); L. Yang and T. S. Rahman, Phys. Rev. Lett. **67**, 2327 (1991).

[9] F. D. Di Tolla, E. Tosatti, and F. Ercolessi, in *Monte Carlo and Molecular Dynamics of Condensed Matter Systems*, edited by K. Binder and G. Ciccotti (SIF, Bologna, 1996), Vol. 49.

[10] C. S. Jayanthi, E. Tosatti, and A. Fasolino, Phys. Rev. B **31**, 470 (1985); C. S. Jayanthi, E. Tosatti, and L. Pietronero, *ibid.* **31**, 3456 (1985).

[11] N. Marzari, D. Vanderbilt, and M. C. Payne, Phys. Rev. Lett. **79**, 1337 (1997).

[12] N. Marzari, Ph.D. thesis, University of Cambridge (1996), available at http://www.physics.rutgers.edu/ in ~marzari/preprints.

[13] A. De Vita, Ph.D. thesis, University of Keele, 1992.

[14] C.-L. Fu and K.-M. Ho, Phys. Rev. B **28**, 5480 (1983); S. de Gironcoli, Phys. Rev. B **51**, 6773 (1995).

[15] M. Methfessel and A. T. Paxton, Phys. Rev. B **40**, 3616 (1989).

[16] M. R. Pederson and K. A. Jackson, Phys. Rev. B **43**, 7312 (1991).

[17] G. N. Kamm and G. A. Alers, J. Appl. Phys. **35**, 327 (1964).

[18] M. P. Allen and D. J. Tildesley, *Computer Simulation of Liquids* (Oxford University Press, Oxford, 1987), Sect. 7.4.3.

[19] E. V. Zarochentsev, S. P. Kravchuk, and T. M. Tarusina, Sov. Phys. Solid State **18**, 239 (1976), and references therein.